INL/JOU-23-70901-Revision-0

Gamma Radiolysis of Phenyl-Substituted TODGAs: Part II

July 2023

Christopher A Zarzana, Jack McAlpine, Aspen Vandevender, Cathy Rae, Andreas Wilden, Michelle Hupert, Andrea Strk, Mudassir Iqbal, Willem Verboom, Bruce J. Mincher, Gary Groenewold, Giuseppe Modolo

Changing the World's Energy Future

Idaho National Laboratory

INL is a U.S. Department of Energy National Laboratory operated by Battelle Energy Alliance, LLC

DISCLAIMER

This information was prepared as an account of work sponsored by an agency of the U.S. Government. Neither the U.S. Government nor any agency thereof, nor any of their employees, makes any warranty, expressed or implied, or assumes any legal liability or responsibility for the accuracy, completeness, or usefulness, of any information, apparatus, product, or process disclosed, or represents that its use would not infringe privately owned rights. References herein to any specific commercial product, process, or service by trade name, trade mark, manufacturer, or otherwise, does not necessarily constitute or imply its endorsement, recommendation, or favoring by the U.S. Government or any agency thereof. The views and opinions of authors expressed herein do not necessarily state or reflect those of the U.S. Government or any agency thereof.

INL/JOU-23-70901-Revision-0

Gamma Radiolysis of Phenyl-Substituted TODGAs: Part II

Christopher A Zarzana, Jack McAlpine, Aspen Vandevender, Cathy Rae, Andreas Wilden, Michelle Hupert, Andrea Strk, Mudassir Iqbal, Willem Verboom, Bruce J. Mincher, Gary Groenewold, Giuseppe Modolo

July 2023

Idaho National Laboratory
Idaho Falls, Idaho 83415

http://www.inl.gov

Prepared for the
U.S. Department of Energy
Under DOE Idaho Operations Office
Contract DE-AC07-05ID14517

Gamma Radiolysis of Phenyl-Substituted TODGAs: Part II

Christopher A. Zarzana*[a], Jack McAlpine[a,b], Andreas Wilden[c], Michelle Hupert[d], Andrea Stärk[d], Mudassir Iqbal[e], Willem Verboom[f], Aspen N. Vandevender[a,b], Bruce J. Mincher[a], Gary S. Groenewold[a], Giuseppe Modolo[c]

* Address reprint requests to Christopher A. Zarzana, Idaho National Laboratory, P.O. Box 1625, Idaho Falls, ID 83415-3531, United States of America. E-mail: christopher.zarzana@inl.gov.

[a] Idaho National Laboratory, Idaho Falls, ID 83415, United States of America.

[b] University of Idaho, Moscow, ID 83844, United States of America.

[c] Forschungszentrum Jülich GmbH, Institut für Energie- und Klimaforschung - Nukleare Entsorgung (IEK-6), 52428 Jülich, Germany.

[d] Forschungszentrum Jülich GmbH, Zentralinstitut für Engineering, Elektronik und Analytik (ZEA-3), 52428 Jülich, Germany.

[e] Department of Chemistry, School of Natural Sciences (SNS), National University of Sciences and Technology (NUST), Islamabad, 44000, Pakistan

[f] Laboratory of Molecular Nanofabrication, Mesa+ Institute for Nanotechnology, University of Twente, 7500 AE Enschede, The Netherlands.

Abstract

The radiolytic degradation chemistry of three phenylated analogs of N,N,N',N'-tetraoctyl diglycolamide (TODGA) was investigated: 2-(2-(di-n-octylamino)-2-oxoethoxy)-N,N-di-n-octyl-2-phenylacetamide (PhTODGA), which has a phenyl substituent bound to a central methylene, 2-(2-(di-n-octylamino)-2-oxo-1-phenylethoxy)-N,N-di-n-octylpropanamide (PhMeTODGA), which also contains a methyl substituent bound to the methylene on the other side of the ether moiety, and, 2-(2-N-n-hexyl-N-phenylamino)-2-oxoethoxy)-N-n-hexyl-N-phenylacetamide (DHDPDGA), which has phenyl substituents located on the amide groups instead of the central methylenes. In Part II of this series of papers, radiolytic degradation products were identified after separation with liquid chromatography by High Resolution, Accurate-Mass mass spectrometry and collision-induced dissociation. At least twenty-two radiolytic degradation products were identified for PhTODGA, twenty-nine for PhMeTODGA, and over three dozen for DHDPDGA. The suite of radiolytic degradation products of these three investigated ligands was significantly larger than has been reported for previously studied diglycolamides, owing to their asymmetric nature, and to the identification of several new degradation mechanisms, including addition of methyl, hydroxyl, and nitrogen oxide radicals, that have not been previously reported for diglycolamides. Degradation products that contained addition of a NO_2 or NO_3 group were particularly prevalent for DHDPDGA, likely due to the phenyl side-groups. Several of these newly observed mechanisms do not appear to depend on the presence of the phenyl groups, suggesting these novel mechanisms may apply to other diglycolamides.

Keywords: Radiolysis, Radical chemistry, TODGA, diglycolamides

Introduction

The growing consequences of anthropogenic climate change have resulted in increased interest in nuclear power, which can provide carbon-free generation of energy.[1] However, management of used nuclear fuel remains a challenge to large-scale deployment of nuclear reactors in many places.[2] Geologic requirements for storage repositories limit the number of sites available, and thus the capacity, for storage of the final waste-form products of nuclear fuel cycles. Social and political resistance to repository construction further limits overall storage capacity.[3] Thus, technologies that can increase the efficiency of use of limited geologic storage space can enable an increase in the size of a nation's nuclear power generation capacity.[4–7]

Partitioning and transmutation (P&T) schemes are of interest as one way to reduce the total volume of radioactive material that requires deep geologic storage.[7,8] Briefly, P&T schemes aim to extract the bulk uranium, plutonium, and neptunium out of the used nuclear fuel. The raffinate left after this extraction step contains fission products, lanthanides (Ln), and the minor actinides (An) americium (Am) and curium (Cm). As the heat from the radioactive decay of americium is the dominant contribution to waste-form heat load from approximately 200 to 2000 years after removal from a reactor,[4] one central aim of the concept of P&T is removal of the minor actinides from the remainder of the used fuel.[7] Once removed, the minor actinides can be burned in a fast neutron spectrum reactor, yielding more energy and converting the minor actinides into short-lived fission products.[9,10]

Ligand molecules for used nuclear fuel separation processes must operate in the extreme environment of high acidity and high radiation field, which results in the radiolytic degradation of the ligand molecules.[11–14] The degradation of the separation ligands can diminish the efficiency of a separation process both through the loss of the separation ligands and through the formation of degradation products that can have a deleterious effect on the separation process. Thus, elucidation of ligand radiolytic degradation mechanisms is critical to development of novel ligand molecules for used nuclear fuel separation.

The diglycolamides (DGAs) have emerged as a class of candidate ligand molecules for separation of the minor An and Ln from the rest of the components of used nuclear fuel, due to high extraction efficiencies for the minor An and Ln and high enough radiation resistance to be industrially useful.[15,16] Several reports have studied DGA molecules with alkane side-chains and substitutions adjacent to the central ether oxygen, with attention to identification of their radiolytic degradation products and mechanisms in alkane diluents, including *N*,*N*,*N'*,*N'*-tetraoctyl diglycolamide (TODGA),[17–20] *N*,*N*,*N'*,*N'*-tetra(2-ethylhexyl) diglycolamide (TEHDGA),[18,21] methyl tetraoctyldiglycolamide, (MeTODGA),[22] dimethyl

tetraoctyldiglycolamide (Me_2TODGA),[22] *N*,*N*-didodecyl-*N'*,*N'*-dioctyldiglycolamide (D^3DODGA),[23] and dimethyl tetradectyldiglycolamide (mTDDGA).[24] The conclusion of these studies is that the primary radiolytic degradation products of the DGAs result from cleavage of the central bonds of the molecule, followed by capping with either a hydrogen ($H^{\bullet}$) or hydroxyl ($^{\bullet}OH$) radical. Other identified degradation products could form as the result of reactions with solvent molecules,[19,20,23,24] or from elimination of molecular hydrogen.[19,20,24] It is believed that the hydrogen bonds adjacent to the central ether oxygen are the most susceptible to radical attack.[19,20,24–26]

The presence of radiolytic degradation products can affect a separation process in numerous ways. Galánet al. studied the extraction efficiency of several TODGA degradation products.[27] 2-(2-(Dioctylamino)-2-oxoethoxy)acetic acid showed distribution ratios less than one for americium and europium, which means its presence would inhibit extraction, possibly due to enhanced solubility in the aqueous phase from the presence of the carboxylic acid group. N,N-Dioctyl-2-(2-(octylamino)-2-oxoethoxy)acetamide had distribution ratios greater than one for Am and Eu, meaning it would enhance extraction. This is likely because it is structurally very similar to TODGA, as it is the result of the loss of a single side chain. 2-Hydroxy-N,N-dioctylacetamide also showed distribution greater than one. Hubscher-Bruder et al. further investigated the trivalent actinide/actinide extraction efficiency of 2-hydroxy-N,N-dioctylacetamide by comparing it to its methyl ester analog, which suggested the presence of the hydroxyl group contributes to enhanced extraction.[28] 2-Hydroxy-N,N-dioctylacetamide and 2-hydroxy-N,N-dioctylpropanamide also had zirconium distribution ratios greater than one. Other investigated degradation products of TODGA and MeTODGA, especially those with monoamide structures, show poor extraction for the trivalent actinides and minor actinides but had distribution ratios higher than one for other metal cations that

would be present in the feed of used nuclear fuel separation processes, such as zirconium, molybdenum, palladium, and copper.

Elucidation of the influence of DGA molecular structure on radiolytic degradation rates and mechanisms is important for developing new molecules for improved separation processes. In Part I of this manuscript series, we report on the influence of phenyl substitution on the rates of gamma-radiation-induced degradation of TODGA analogs.[29] Here we report on the radiolytic degradation product chemistry of the phenyl-substituted analogs. As in Part I, we investigated two phenyl-substituted versions of TODGA: 2-(2-(di-*n*-octylamino)-2-oxoethoxy)-*N*,*N*-di-*n*-octyl-2-phenylacetamide (trivially, *N*,*N*,*N'*,*N'*-tetraoctyl phenyldiglycolamide, PhTODGA, Figure 1a), and 2-(2-(di-*n*-octylamino)-2-oxo-1-phenylethoxy)-*N*,*N*-di-*n*-octylpropanamide (trivially, *N*,*N*,*N'*,*N'*-tetraoctyl phenylmethyldiglycolamide, PhMeTODGA, Figure 1b), which have phenyl groups located in proximity to the central ether oxygen of the DGA backbone. We also investigated the radiolytic degradation product chemistry of 2-(2-*N*-*n*-hexyl-*N*-phenylamino)-2-oxoethoxy)-*N*-*n*-hexyl-*N*-phenylacetamide (trivially, *N*,*N'*-dihexyl-*N*,N'-diphenyl diglycolamide, DHDPDGA, Figure 1c), which has phenyl and hexyl side-groups but no ether-adjacent substitutions.

Actual used fuel separation processes may use industrial hydrocarbon mixtures such as kerosene or hydrogenated tetrapropene (TPH),[9,10] and contain can contain co-extractants and other molecules like phase modifiers. Additionally, real processes likely operate at elevated temperature due to the heat from fission product decay. There is evidence that radiolysis of separation ligands could be different in the more complicated conditions expected in a separations process than in the simplified conditions typically used for radiolysis studies. For example, irradiations of air-sparged TODGA-containing solvents show some new degradation products that were not previously identified, though most of the identified

degradation products were the same as have been observed prior.[30]However, given the wide range of potential conditions, and the complexity that brings, most DGA radiolysis studies have been conducted under simplified conditions, typically static irradiations in *n*-dodecane, and in *n*-dodecane in contact with nitric acid-containing aqueous phases.[18,22–24,31] To enable comparison to these prior studies, we have utilized these same kinds of conditions.

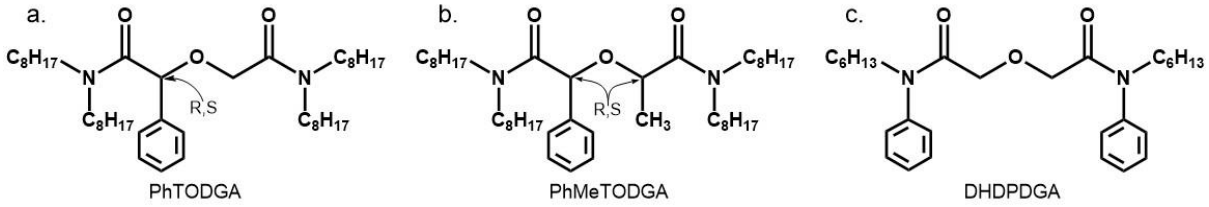

Figure 1: Structures of a) PhTODGA, b) PhMeTODGA, and c) DHDPDGA. Note that PhTODGA has a stereogenic carbon center, yielding two enantiomers (labeled R,S in the figure), and that PhMeTODGA has two stereogenic carbons, yielding four stereoisomers.

Experimental

Ligand preparation

PhMeTODGA and PhTODGA were prepared following the methodology described by Iqbal et. al.[32] TODGA (~98% purity) was purchased from Marshallton Research Laboratories, Inc. (King, North Carolina, USA, http://www.marshalltonlabs.com), and used without further purification. *N,N'*-di-*n*-hexyl-*N,N'*-diphenyl diglycolamide (DHDPDGA) was synthesized under Schotten-Baumann conditions according to the general procedure described in Leoncini et al.[33] Nuclear magnetic resonance peaks of the product supporting identity are provided in Part I.[29]

Gamma-Ray irradiation

Detailed gamma irradiation conditions are provided in Part I, and have been chosen for consistency with previous studies of diglycolamide radiolysis.[18,22–24,31] Briefly, samples of

PhMeTODGA, PhTODGA, and DHDPDGA were irradiated as 0.05 M solutions in *n*-dodecane either as the pure organic phase, or in contact with either 0.1 M HNO_3 or 3.0 M HNO_3. Biphasic samples were mixed and allowed to sit for 24 hours at room temperature (20-23 °C) to ensure equilibration prior to irradiation. in a Nordion GammaCell 220E (Ottawa, Canada) ^{60}Co source, with a centerline sample chamber dose rate of 4.5 kGy h^{-1}, as determined by decay corrected Fricke dosimetry.[34,35]

UHPLC-ESI-MS

PhMeTODGA and PhTODGA Degradation Product Analysis

Irradiated PhMeTODGA samples in *n*-dodecane were diluted in Optima® LC/MS 2-propanol (Fisher Scientific, Pittsburgh, PA, USA) prior to analysis to generate a concentration in the low micromolar (μM) range. The diluted samples were analyzed using a Dionex (Sunnyvale, CA, USA) ultra-high-performance liquid chromatograph (UHPLC) with an Ultimate 3000 RS pump, 3000 RS autosampler, 3000 RS column compartment and a 3000 RS diode-array detector, coupled to a Bruker (Billerica, MA, USA) microTOFQ-II electrospray ionization (ESI) quadrupole time-of-flight mass spectrometer with Hystar 3.2 software.

The chromatographic separation was achieved using 5 μL injections on a Kinetex 1.7 μm particle size, EVO-C18 stationary phase, 50 mm × 2.1 mm column (Phenomenex, Torrance, CA, USA) held at 50 °C. The aqueous component was Optima® LC/MS water with 0.1% v/v formic acid (Fisher Scientific, Pittsburgh, PA), and the organic component was Optima® LC/MS 2-propanol. A 25-minute isocratic mobile phase profile was initially used to separate the irradiated PhMeTODGA solutions, with a flow rate of 300 μL/min and a 59% organic composition. A 10-minute gradient mobile phase profile was used to separate the irradiated PhTODGA solutions. The mass spectrometer conditions were: capillary: 4.5 kV, positive

mode; temp.: 220 °C; nebulizer gas and dry gas were both N_2, nebulizer pressure: 0.4 bar; dry gas flow rate: 9 L/min. The mass spectrometer was operated using standard Bruker "tune low" and "tune wide" tuning parameters. Each sample was injected three times.

DHDPDGA Degradation Product Identification

Degradation product analysis was performed at Forschungszentrum Jülich (FZJ) using an Agilent 1200 HPLC coupled to a LTQ FT Ultra™ (Thermo Fisher Scientific, Bremen, Germany) hybrid linear ion trap Fourier-Transform Ion Cyclotron Resonance mass spectrometer. The Agilent 1200 HPLC system consisted of a binary pump system, an autosampler, a thermostated column compartment at 35°C and a diode-array detector (Agilent, Waldbronn, Germany). The mass spectrometer was first tuned and calibrated in the positive mode following the standard optimization procedure for all voltages and settings: Source Type: ESI: Ion Spray Voltage 3.8 kV, Capillary Voltage 37 V, Tube Lens: 130 V; Capillary Temp 275°C, Sheath Gas Flow: 60 a.u. Mass spectra were recorded in full scan mode from 100 to 1000 Da with a resolution of 100,000 at m/z 400. All data were processed using the Xcalibur™ software 2.0 (Thermo Fisher Scientific, Bremen, Germany). Only m/z ratios with a mass deviation <1 ppm to the calculated chemical composition were considered.

Results and Discussion

Degradation Product Identification

The ion chromatogram of 0.05 M PhMeTODGA after irradiation to 500 kGy absorbed dose in contact with an aqueous solution of 3.0 M HNO_3 is shown in Figure S1. There are more than two dozen peaks, most of which have been assigned as degradation products of PhMeTODGA. Compound numbers are assigned based on the retention order of the degradation products for each of the phenylated DGAs. There are a few products detected in the PhMeTODGA samples that have no analog in the PhTODGA samples, so some compounds that are proposed to have the same structures for the PhMeTODGA and PhTODGA samples have different compound numbers. Proposed structures for these degradation products were derived from exact mass measurements (PhMeTODGA: Table S1, PhTODGA: Table S2, and DHDPDGA: Table S3), interpretation of collision-induced dissociation (CID) tandem mass spectrometry (MS^2) spectra, and logical bond cleavages and capping reactions of the parent DGA. CID tandem mass spectra and proposed fragmentation schemes explaining those spectra can be found in the Supplementary Information (PhMeTODGA: Figure SA1 to Figure SA29 and Scheme SA1 to Scheme SA28, PhTODGA: Figure SB1 to Figure SB22 and Scheme SB1 to Scheme SB22, with Figure and Scheme numbers corresponding to compound number). There was less DHDPDGA material available, so CID spectra were only obtained for a few degradation products (Figure SC1 through Figure SC3, and Scheme SC1 through Scheme SC3). Proposed structures for DHDPDGA degradation compounds with no CID data were derived from exact masses (Table S3) and logical bond cleavages. PhMeTODGA has two chiral centers, and thus two diastereomers that can be chromatographically resolved. Therefore, degradation products of PhMeTODGA that retain these two chiral centers will also have two sets of two enantiomers, and will result in two chromatographic peaks, which have identical *m/z* and CID spectra.

Where identified, these compounds have been labeled with *a* or *b* (PhMeTODGA Compounds 6a and 6b, for example in Figure 2), indicating retention order, as the specific stereochemistry cannot be identified using mass spectrometry.

Irradiation of DHDPDGA resulted in even more radiolytic degradation products than PhMeTODGA and PhTODGA, particularly those which would result from addition of NO_2 and NO_3 groups. As with PhMeTODGA and PhTODGA, proposed structures of the degradation products are derived from exact mass measurements (Table S3) and logical bond cleavages and capping reactions of the parent DGA. However, because of the limited amount of sample, we were unable to collect CID spectra for many of the compounds detected in the DHDPDGA samples. For DHDPDGA, several chromatographic peaks with different retention times were observed with the same *m/z* ratios, which could correspond to more than one chemical structure. Without CID data, the mass spectrometer does not provide structural data, only formula. Therefore, these are proposed structures, informed by the radiolytic fragmentation chemistry of PhMeTODGA and PhTODGA, but further investigation of these compounds would be required to definitively identify and characterize them.

Radiolytic degradation pathways, and product dose profiles

Mixtures formed from radiolysis of PhTODGA, PhMeTODGA and DHDPDGA contain a plethora of compounds, most of which are formed from radiolysis reactions, although some are also formed by purely chemical means. Products were identified from cleavage of nearly every bond in the core of the diglycolamide molecules – only the phenyl, pendant methyl, carbonyl, and bonds internal to the *N*-*n*-alkyl groups were spared. Radiolysis product identification was based on elemental composition derived from accurate mass

measurements, and from CID spectra. Radiolysis pathways are summarized for PhMeTODGA in Figure 2 and Figure 4. Proposed radiolysis pathways and degradation product structures for all three compounds studied here are also reported in the Supplementary Information, Figure S2 through Figure S5, and measured compounds in Table S1 through Table S4. Here, the radiolysis product identities are discussed in the context of the DGA bond cleavage, initially forming larger radicals that are capped with low molecular weight radicals that are also formed in the radiolysis experiments. Identification of the radiolysis reactions provides a starting point for the development of a comprehensive understanding of compound degradation, even though a quantitative description of competing degradation reactions is currently unavailable, the latter on account of unknown (and varying) ionization efficiencies under ESI conditions. The chromatographic peak area for a given compound is proportional to the compound concentration even though the conversion factor is unknown due to unknown ionization efficiencies. Thus, the signal areas for a given compound can be compared between different irradiation conditions, providing some information on degradation mechanisms.

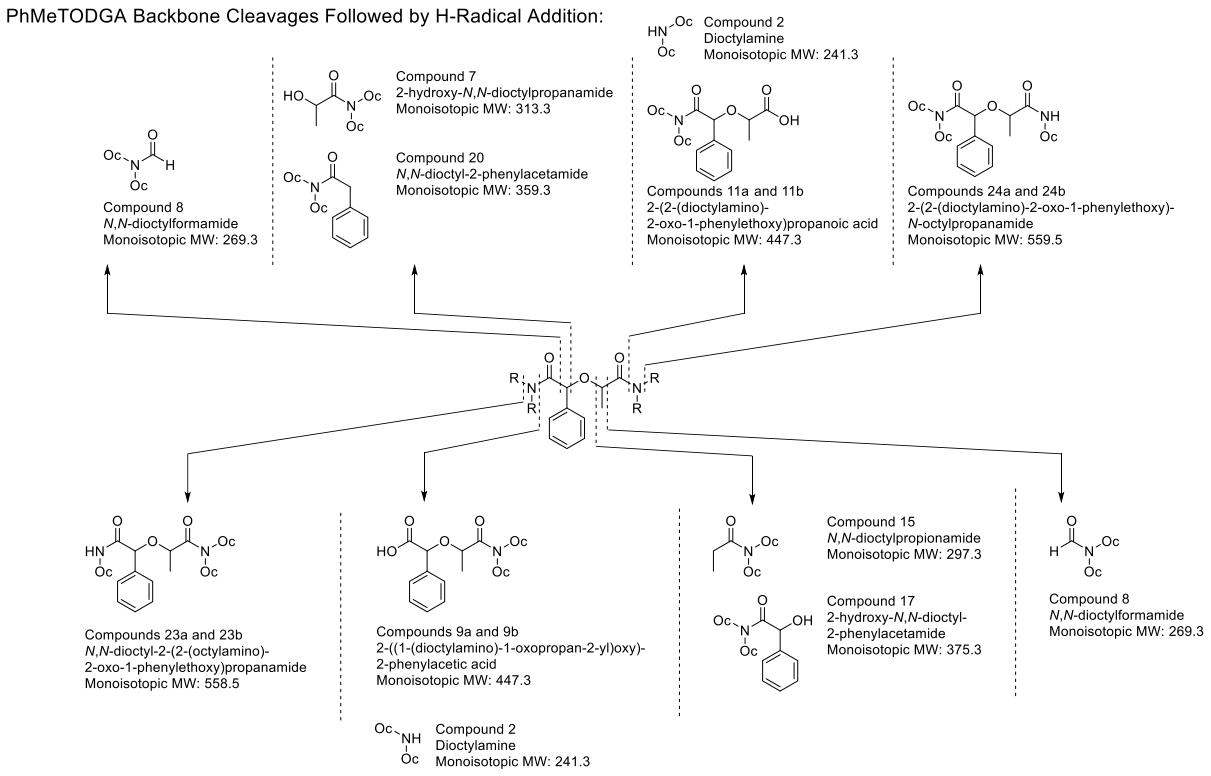

Figure 2: Proposed structures and formation mechanism classification of PhMeTODGA degradation products arising from cleavage of backbone bonds. R groups are *n*-octyl (C_8H_{17}).

The abundance of the degradation products as a function of dose is also informative, displaying two general profiles: a) increasing in abundance at low dose, and then falling at high doses, and b) only increasing in abundance as dose increases, at least to the maximum absorbed dose used in this work. The radiation-induced radicals that are responsible for destruction of the parent DGA and production of the degradation products can also react with the degradation products, inducing secondary reactions. The likelihood of occurrence of these reactions increases with increasing degradation product concentration. Thus, degradation products that exhibit the first abundance profile (increasing at low dose followed by a roll-off or decrease at high dose) are likely to have been formed with high efficiency, resulting in sufficient concentration at high dose to undergo radiolytic degradation. Degradation products exhibiting the second dose profile (increasing abundance as a function of dose) are likely to

be present in low concentrations, either as the result of low efficiency formation mechanisms or because they are formed from radiolytic degradation of primary radiolysis products, as opposed to being directly formed from radiolytic degradation of the parent DGA.

Compounds from C_{alkyl}—N_{amide}, and C_{phenyl}—N_{amide} Cleavages

In the PhTODGA and PhMeTODGA experiments, cleavage of the C_{octyl}—N_{amide} bonds produces mono-N-octyl amido derivatives, by initial formation of a nitrogen-centered radical that is capped with H•. Both the phenylated and non-phenylated sides of PhMeTODGA react in this fashion forming two sets of *des*-octyl derivatives, that show up as enantiomeric pairs in the HPLC/MS analysis (Figure 2, compounds 23a,b, 24a,b). PhTODGA displays very similar behavior, producing *des*-octyl compounds 19 and 20 in Figure S3. The radiolytic abundance profiles of these compounds suggest that they are products of primary reactions that subsequently undergo secondary radiolysis reactions: the profiles increase sharply over the first 150 kGy of gamma dose, before plateauing at about 300 kGy and then decreasing at higher doses (Figure 3, Figure S6 through Figure S9).

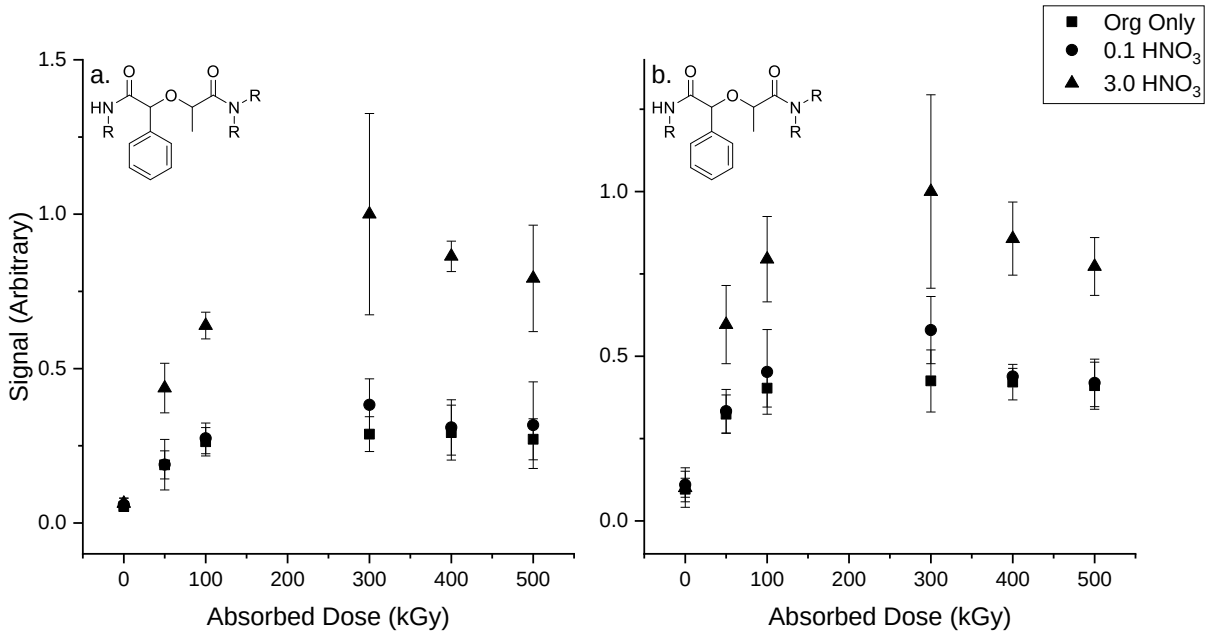

Figure 3: Normalized signal *vs.* absorbed dose for (a) PhMeTODGA compound 23a, and (b) PhMeTODGA compound 23b (enantiomeric pairs, see Figure 2).

The abundance increase with dose was greatest for the experiments conducted in 3 M HNO_3, suggesting that this radiolysis mechanism is facilitated by the acidic environment; increase in abundance of amide products in the presence of nitric acid was also observed for previously studied DGAs.[13,16] This conclusion is consistent with the idea that radiolysis is accelerated by amide functional groups that are protonated or partially protonated, weakening neighboring bonds. The decrease in abundance at doses > 300 kGy is attributed to secondary radiolysis processes, i.e., converting the mono-N-octylamido compounds to other derivatives.

The *des*-octyl derivatives of PhMeTODGA undergo a second octyl• cleavage/H• capping reaction to furnish phenylmethyl-*N*-octyl-*N'*-octyl diglycolamide (Figure 4: compounds 6a,b), and PhTODGA does the same thing to form methyl-*N*-octyl-*N'*-octyl diglycolamide (Figure S3: compound 6). The radiolysis profiles of these compounds display an increase in abundance as dose increases, consistent with the hypothesis that they are being formed as secondary radiolysis products (PhMeTODGA, Figure S10: compounds 6a and b; PhTODGA, Figure S11: compound 6). If the octyl• cleavage/H• capping reaction was undirected, loss of

an additional side-chain from PhMeTODGA compounds 23a, 23b, 24a, and 24b would be expected to result in three degradation products: one compound with two octyl side-chains on the phenyl-side amide and none on the methyl-side amide, one compound with no octyl side-chains on the phenyl-side amide and two on the methyl-side amide, and one compound with one side-chain on each side of the molecule, resulting in six peaks because of the two stereogenic carbons. However, only two peaks (Figure 4: compounds 6a and 6b) are present, and the CID spectra of the two indicate that there are octyl groups on both sides of the molecule. Thus, loss of one octyl chain from an amide appears to stabilize that amide against loss of a second.

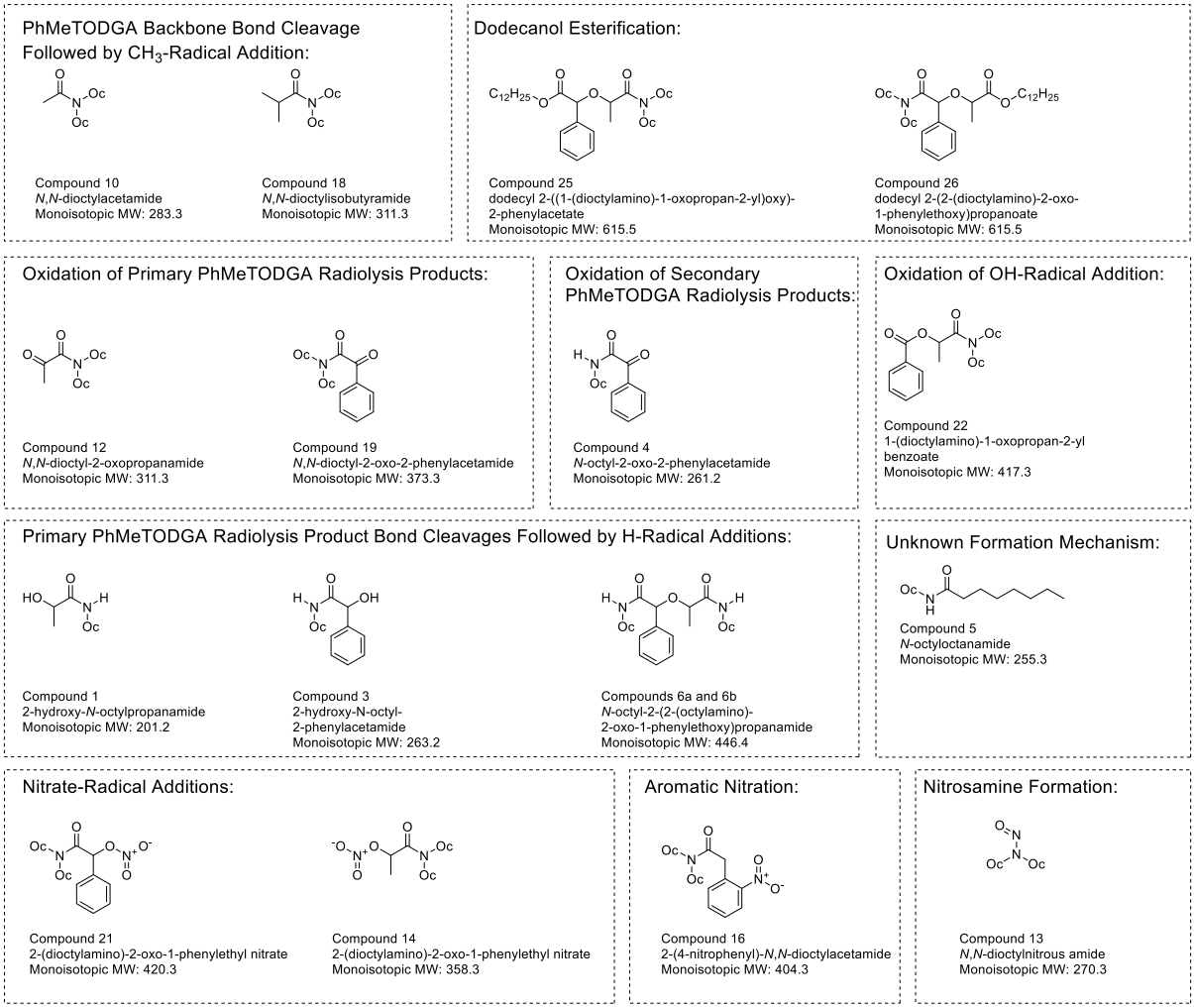

Figure 4: Radiolysis pathways for PhMeTODGA involving proposed pathways other than cleavage of a backbone bond followed by capping with a hydrogen radical.

DHDPDGA undergoes analogous reactions. Elimination of hexyl• / H• capping results in an *N*-hexyl-*N*-phenyl-*N*'-phenyl derivative (Figure S4, compound 1); the chromatographic intensity increases by an order of magnitude over the first 50 kGy in experiments conducted in organic-only, and organic-0.1 M HNO_3 contacted environments (Figure S39). Beyond 50 kGy, intensities continue to increase but at a more modest rate. A significant amount of this compound is also observed in the analyses of the third phase that was formed.[29] Compounds originating from cleavage of a phenyl moiety behave in a practically identical fashion (Figure S4, compound 2, and Figure S40).

DHDPDGA also undergoes serial hexyl• loss/H• capping followed by phenyl• loss/H• capping to generate a *N*-hexyl-*N'*-phenyl diglycolamide, which increases in intensity by two orders of magnitude in organic-only experiments but does not appear to be generated from radiolysis of HNO_3-contacted solutions (DHDPDGA compound 11, Figure S41). Serial elimination of hexene and a H•, followed by capping with O_2N• or O_2NO• also occurs (Figure S42 and Figure S43). These products are principally observed in the organic phase of the HNO_3-contacted experiments; however, at high doses, the nitrato compound is also observed in abundance in the third phase.

Compounds from N_{amide}—$C_{C=O}$ Cleavages

Homolytic cleavage of the N_{amide}—$C_{C=O}$ would initially generate a dioctylamino radical, and a carbonyl radical. In the PhTODGA and PhMeTODGA experiments, capping the amino radical with H• furnishes dioctylamine from both sides of these molecules, consistent with the abundant peak observed in the chromatogram at 3.3 min. (compound 2 in Figure 2 and Figure S3). Capping the $C_{C=O}$ radical occurs by reaction with hydroxide radicals (HO•), generating carboxylic acid derivatives, albeit in low abundance. These are compounds 9a,b and 11a,b from PhMeTODGA (Figure 2), and compounds 8 and 10 from PhTODGA (Figure

S3). Either H_2O or HNO_3 must be required for formation of the carboxylic acid products, and both are present in these experiments. However, it is surprising that products from HO• capping are not observed for the other initially formed radicals. This suggests that the reaction between the HO• radical and the amide radical is kinetically or energetically favored, while the reactions between the HO• radical and other DGA radicals are not. Curiously, products of H• capping of the carbonyl radicals to form aldehyde derivatives are not observed in the PhTODGA or PhMeTODGA experiments.

The radiolytic profile for di-*n*-octylamine shows a slow increase in abundance up to ~ 50 kGy, followed by a slow increase to 300 kGy and constant values thereafter – this is observed for experiments conducted in *n*-dodecane, and in *n*-dodecane contacted with 0.1 M HNO_3 (Figure S14). The profile from the experiment contacted with 3.0 M HNO_3 is dramatically different: abundance increases dramatically up to 400 kGy, and then decreases. The production of di-*n*-octylamine is clearly augmented by the presence of abundant acid, weakening the amide bonds as a result of protonation as suggested above. The fact that the abundance of di-*n*-octylamine decreases at 500 kGy indicates secondary reactions, and in fact *N*-nitroso-di-*n*-octylamine (Figure 2, compound 13) is formed from PhMeTODGA, but not until very high doses have been delivered (Figure S18).

The abundances of the carboxylic acid derivatives (e.g. compounds 9a,b and 11a,b from PhMeTODGA, Figure 2, and compound 8 from PhTODGA, Figure S3) also increase rapidly at low dose, peaking at ~ 100 kGy before undergoing significant decreases (Figure S12, Figure S13, and Figure S15). The abundance decrease at higher doses indicates secondary reactions, and compounds resulting from esterification with *n*-dodecyl moieties are observed (PhMeTODGA Figure 4, compounds 25 and 26; PhTODGA, Figure S3, compounds 21 and 22). However, the radiolysis profiles for the dodecyl esters are consistent with primary degradation products (Figure S16 and Figure S17). Significantly, the ester derivatives are

only observed in the 3.0 M HNO_3 environments, where a substantial amount of di-*n*-octylamine was generated.

In the DHDPDGA experiments, N_{amide}—carbonyl cleavage initially forms a carbonyl radical that reacts with H• to form a DGA aldehyde derivative (Figure S4, compound 8); this contrasts with the phenyl TODGA molecules, where HO• capping is observed. In the organic-only, and 0.1 M HNO_3 experiments, the intensity of the chromatographic signal rises two orders of magnitude over a dose of 500 kGy, with most of the increase occurring in the first 100 kGy (Figure S44).

N-hexyl-phenylamine is also observed in high abundance in the majority of the DHDPDGA radiolysis environments (Figure S45), formed from H• capping of the initially formed amino radical. This reaction product is analogous to those seen in the phenyl TODGA compounds. In the organic-only environment, it is at reasonably high abundance before irradiation was initiated, indicating that it is formed by purely chemical means. Upon irradiation, its abundance increases by about a factor of five at 300 kGy, before decreasing. A similar pattern was seen in both phases of the 0.1 M HNO_3-contacted experiment. *N*-hexyl-phenylamine abundance does not vary significantly in the organic phase of the 3 M HNO_3-contacted experiment. The initially formed amino radical is also capped by H_3C•, generating *N*-hexyl-*N*-methyl-phenylamine (Figure S46). This compound is only observed with any abundance in the organic-only experiment at high doses.

Nitrato, nitro and nitroso derivatives of *N*-hexyl-phenylamine are also formed in the DHDPDGA experiments (Figure S5, compound 10 + NO_3, compound 10 + NO_2, and compound 10 + NO, respectively). Serial elimination of H• from the phenyl moiety, followed by capping with O_2NO•, O_2N• and ON• are expected to generate nitratophenyl-, nitrophenyl-, and *N*-hexyl-(nitrosophenyl)amine derivatives, structures consistent with CID spectra. *N*-

Hexyl-(nitratophenyl)amine abundance increases by more than two orders of magnitude in the aqueous phase of the 0.1 M HNO_3-contacted experiment over the first 100 kGy of gamma dose, then decreases at doses > 300 kGy (Figure S47) signaling the onset of secondary radiolysis reactions. This compound is also formed in abundance in the organic phase of this experiment.

N-Hexyl-(nitrophenyl)amine is observed in abundance in the DHDPDGA-containing organic phases of both the 0.1 M and 3 M HNO_3-contacted experiments at zero gamma dose, and its abundance increases with increasing dose in the organic and aqueous phases of the 0.1 HNO_3-contacted experiment. This indicates that it is formed by chemical means, and also from radiolysis (Figure S48). At the highest doses, abundance decreases, signaling secondary radiolysis reactions. The abundance of *N*-hexyl-(nitrosophenyl)amine also increases significantly with increasing gamma dose for both phases of the 0.1 M HNO_3-contacted, and organic-only experiments (Figure S49). It is abundant at zero dose in the organic phase of the 3 M HNO_3-contacted experiment, indicating that it can be formed in the absence of gamma radiation.

Like the phenyl TODGA molecules, an abundant carboxylic acid derivative is formed from HO• capping of the carbonyl radical from DHDPDGA. This compound is favored in the organic-only experiment and in the third phase but is not nearly as abundant in the more acidic environments (Figure S50). This would seem to rule out a formation reaction that involves HNO_3. The carboxylic acid also undergoes esterification with a dodecyl moiety (Figure S51), which is observed in modest abundance in all three organic environments that were analyzed. The mechanism is not known, but the formation of this compound is consistent with the observation of *n*-dodecyl hydroperoxide (Figure S68.

Nitratophenyl and nitrophenyl derivatives of the DHDPDGA-derived carboxylic acid product are also formed, by serial C_{phenyl}—H cleavage with capping by either O_2NO• or O_2N•. The nitratophenyl derivative is observed in abundance in the organic-only environment, and surprisingly its initial abundance is significant (Figure S52). This suggests that initially its formation is the result of a non-radiolytic, chemical reaction. At 100 kGy, abundance drops, but then rebuilds, suggesting that at higher doses, the nitratophenylacetic acid derivative is also formed by gamma radiolysis. Another nitrogen oxide radical-capped derivative is formed that has a composition consistent with either a nitrophenylacetic acid, or a nitratophenylacetaldehyde (Figure S53). The compound is found in low abundance in all environments and is most prevalent in the third phase at higher gamma doses.

Compounds from $C_{C=O}$—C_{CH2} Cleavage

Radiolytic cleavage of the $C_{C=O}$—C_{CH2} bonds in PhMeTODGA and PhTODGA generates a dioctylamido radical centered on the carbonyl, and another radical centered on the methylene moieties (from either side of the central ether oxygen atom). In the PhMeTODGA experiments, compounds resulting from capping the dioctylamido radical with either H• or H_3C• produce *N*,*N*-di-*n*-octylformamide (Figure 2, compound 8) and *N*,*N*-di-*n*-octylacetamide (Figure 4, compound 10). The presence of the methyl substituent adjacent to the central ether oxygen atom in PhMeTODGA means that *N*,*N*-di-*n*-octylacetamide (Figure 4, compound 10) cannot be formed directly from cleavage of the $C_{C=O}$—C_{CH2} bond followed by hydrogen radical capping. Instead, this compound must be formed either by loss of a CH_3 group from *N*,*N*-dioctylpropionamide (Figure 2, compound 15) or by cleavage of the $C_{C=O}$—C_{CH2} bond followed by capping with a methyl radical (H_3C•). If the acetamide was formed from secondary radiolysis of the propionamide, its abundance *vs.* absorbed dose would be expected to lag behind the abundance *vs.* absorbed dose for the propionamide: the propionamide concentration would need to grow large enough for the rates of a secondary

reaction to become high enough to produce detectable amounts of the acetamide. However, the abundance of the acetamide begins to increase at low absorbed doses, similar to that of the propionamide (Figure S20 and Figure S24, respectively). This suggests that the acetamide is formed by cleavage of the $C_{C=O}$—C_{CH2} bond followed by capping with a methyl radical (H_3C•).

The analogous processes in the PhTODGA experiments furnish the same compounds (Figure S3, compounds 9, 11). The radiolytic profiles show increasing abundances with gamma dose; the formamide derivative continues to increase over the entire dose range, suggesting that it is not susceptible to further radiolysis, and perhaps that it is formed by a secondary radiolysis reaction (Figure S19). In contrast, the acetamide abundances increase to ~ 300 kGy, and then plateau, suggesting that they are reacting further, or that their precursors are being depleted (Figure S20). An interesting observation is that these amide products are favored in the *n*-dodecane- or low acid-contacted environments. Conversely, formation of the formamides is disfavored in the high acid-contacted environments, and generally this is also true for the acetamide derivatives.

The methylene radicals generated by $C_{C=O}$—C_{CH2} cleavage in PhMeTODGA and PhTODGA are not observed to produce compounds by capping with either H• or H_3C•, but instead appear to generate benzoate esters, by oxidation of the methylene radical to furnish a carbonyl vicinal to the central O_{ether} (Figure 2, compound 22 for PhMeTODGA; Figure S3, compound 15 for PhTODGA). The mechanism for formation of these compounds has not been established but is hypothesized to involve initial capping with HO• followed by oxidation to the carbonyl functional group. Both compounds display typical radiolysis behavior, with increasing concentration to 300 – 400 kGy, followed by a decrease resulting from secondary radiolysis reactions (Figure S21).

In DHDPDGA, $C_{C=O}$—C_{CH2} cleavage with H• capping forms *N*-hexyl-*N*-phenylformamide, which is produced prominently in the organic-only, and organic phase of the 0.1 M HNO_3-contacted environments (Figure S4, compound 3). The anticipated companion product, 2-methoxy-*N*-hexyl-*N*-phenylacetamide, is also produced (Figure S4, compound 5). The radiolysis profiles for both compounds show significant increase in abundance over the first 100 kGy of gamma dose in the organic-only, and organic phase of the 0.1 M HNO_3-contacted environments (Figure S54, Figure S55). A phenyl nitration reaction product is observed, generating a *N*-hexyl-*N*-(nitratophenyl)formamide; this compound is observed in multiple environments, but is most favored at high doses in the organic phases of the HNO_3-contacted experiments (Figure S56). An indeterminate oxidation reaction also proceeds together with $C_{C=O}$—C_{CH2} cleavage, producing 2-formoxy-*N*-hexyl-*N*-phenylacetamide (Figure S4, compound 15). The compound is formed over the first 50 kGy in the organic phases of the HNO_3-contacted, and organic-only experiments; at higher doses slow abundance decreases are seen (Figure S57).

Compounds from C_{CH2}—O_{ether} Cleavage

Cleavage of the interior C_{CH2}—O_{ether} bonds produces a variety of products from PhMeTODGA and PhTODGA, commensurate with the reactivity of primary and secondary C-centered radicals, and dangling O radicals that are initially formed. H• capping of the radicals resulting from cleavage on the phenylated side of the molecules produces 2-methyl-*N*,*N*-di-*n*-octyl glycolamide from PhMeTODGA (Figure 2, compound 7), *N*,*N*-di-*n*-octyl glycolamide from PhTODGA (Figure S3, compound 7), and 2-phenyl-*N*,*N*-di-*n*-octylacetamide from both (Figure 2, compound 20, and Figure S3, compound 17). These products display typical profiles in that their abundance maximizes at 300 kGy and then plateaus, which indicates that either they are stable, or that their rate of formation is about the same as their rate of further degradation (Figure S22). In addition, 2-methyl-*N*,*N*-di-*n*-

octylpropanamide is formed by H_3C• capping of the secondary radical from PhMeTODGA (Figure S2, compound 18), on the non-phenylated side of the molecule. The radiolysis profile shows a steady increase in abundance, consistent with formation by a secondary reaction (Figure S26a). An analogous reaction pathway accounts for the formation of *N*,*N*-di-*n*-octyl propanamide from PhTODGA (Figure S3, compound 12), and it displays similar radiolysis behavior (Figure S26b).

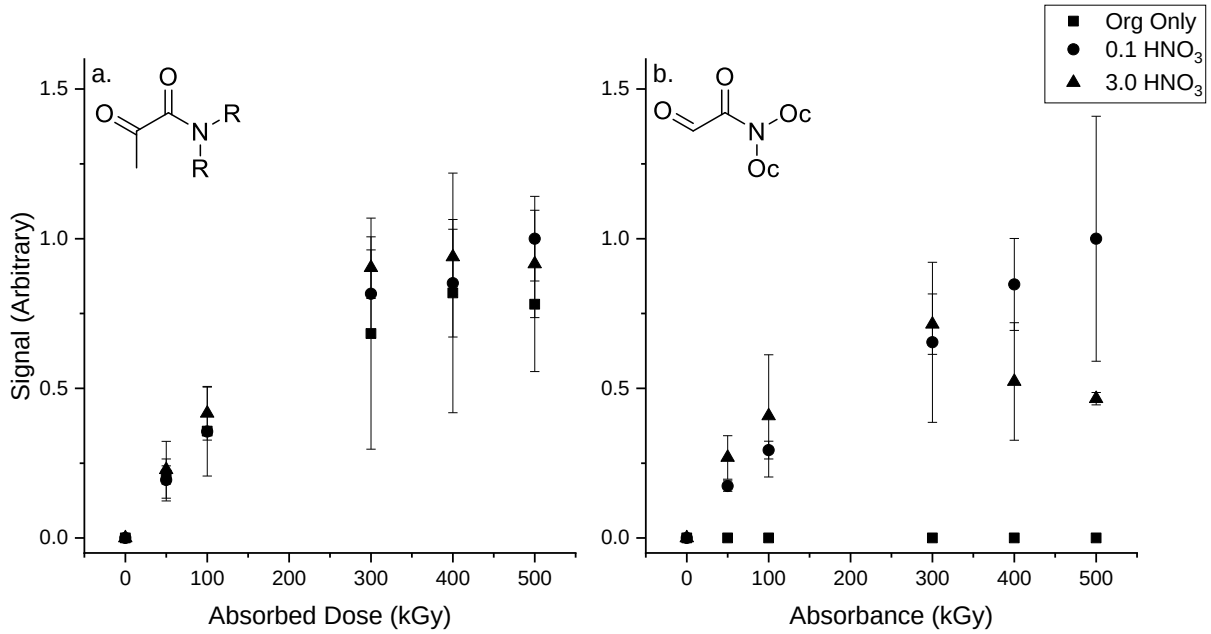

Figure 5: Normalized signal *vs.* absorbed dose for (a) PhMeTODGA, compound 12, and (b) PhTODGA, compound 13. PhMeTODGA compound 12 (a) could be formed from the oxidation of PhMeTODGA compound 7, while PhTODGA compound 13 (b) could be formed from the oxidation of PhTODGA compound 7.

Complementary products are generated from cleavage of the C_{CH2}—O_{ether} on the non-phenylated side of PhMeTODGA and PhTODGA. H• capping of the radicals produced from PhMeTODGA furnish *N*,*N*-di-*n*-octylpropanamide and 2-phenyl-*N*,*N*-di-*n*-octyl glycolamide (Figure 2, compounds 15 and 17, respectively). The same reactions operating on the radicals generated from PhMeTODGA form *N*,*N*-di-*n*-octylacetamide, and 2-phenyl-*N*,*N*-di-*n*-octyl glycolamide (Figure S3, compounds 11 and 14, respectively). Typical radiolysis profiles are

seen for 2-phenyl-*N*,*N*-di-*n*-octyl glycolamide from both parent compounds, with abundance peaking at 300 kGy then decreasing, indicating that this is a primary degradation product (Figure S25). In contrast, the abundances of the acetamide and propanamide derivatives measured in the *n*-dodecane-only environment underwent an initial slow increase, followed by sharp increases after 300 kGy, indicating that these are the products of secondary reactions (Figure S24).

The methylene-centered radicals initially formed from C_{CH2}—O_{ether} cleavage also undergo oxidation: radicals from PhMeTODGA form *N*,*N*-di-*n*-octyl pyruvamide (Figure 2, compound 12) and 2-phenyl-*N*,*N*-di-*n*-octyl glyoxylamide (Figure 2, compound 19). Similar reactions of radicals from PhTODGA generate *N*,*N*-di-*n*-octyl glyoxylamide (Figure S3, compound 13), and 2-phenyl-*N*,*N*-di-*n*-octyl glyoxylamide (Figure S3, compound 16). The abundance of the pyruvamide derivative from PhMeTODGA increases quickly to 300 kGy, and then plateaus, indicating that it is a primary degradation product (Figure 5a, Figure S27a), and the 2-phenyl glyoxylamide products (from PhMeTODGA and PhTODGA) display the same behavior (Figure S28a and b). The abundance of the *N*,*N*-di-*n*-octyl glyoxylamide continues to increase throughout the dose range, suggesting that it may be formed by both primary and secondary mechanisms (Figure 5b, Figure S27b). To our knowledge, there have been no reports of DGA degradation products that would result from the oxidation of alcohol-containing degradation products. While formation of PhMeTODGA compound 19 and PhTODGA compound 16 could be enabled by the proximity of the hydroxide group to a phenyl moiety, analogs of PhMeTODGA compound 12 and PhTODGA compound 13 should occur for other studied DGAs (TODGA, T(EH)DGA, MeTODGA, Me_2TODGA, and D^3ODGA).

The radiolysis products that were produced from C_{CH2}—O_{ether} cleavage and H• capping in PhMeTODGA and PhTODGA subsequently undergo a serial C_{octyl}—N_{amide} cleavage/H•

capping, to produce mono-*N*-octyl versions of the glycolamide derivatives: 3-methyl-*N*-octyl glycolamide from PhMeTODGA (Figure 2, compound 1), *N*-octyl glycolamide from PhTODGA (Figure S3, compound 1), and 2-phenyl-*N*-octyl glycolamide from both parent compounds (compound 3 in both Figure 2 and Figure S3). Generally, these products continue to increase with increasing dose in experiments conducted in *n*-dodecane-only or dilute acid-contacted environments (Figure S29, Figure S30). This is consistent with the notion that these are secondary reactions. When conducted in contact with 3.0 M HNO_3, abundances peak at 300 kGy, then decrease, suggesting that the presence of acid facilitates radiolytic degradation of these compounds. Octyl• cleavage / H• capping also occurs from the compounds that were oxidized, forming 2-phenyl-*N*-octyl glyoxylamide (compound 4 in both Figure 2 and Figure S3). The radiolysis profiles show that this process is favored in the acid-contacted environments, with abundances of the products increasing throughout the 500 kGy dose range, whereas the abundances peak and plateau in the *n*-dodecane-only environments (Figure S31).

Nitration of the radicals initially formed from C_{CH2}—O_{ether} cleavage in PhMeTODGA and PhTODGA also occurs. These reactions form 2-nitrato-2-phenyl-*N*,*N*-di-*n*-octylacetamide from both PhMeTODGA and PhTODGA (Figure 4, compound 21 and Figure S3, compound 18, respectively). 2-Nitratopropanamide is also formed from PhMeTODGA (Figure 4, compound 14). These reactions only occur in the 3.0 M HNO_3-contacted environments. The abundances peak at 300 kGy in the radiolysis profiles of all three compounds, then remain static or undergo slow decreases at higher doses (PhMeTODGA compound 21 and PhTODGA compound 18: Figure S32; PhMeTODGA compound 14: Figure 6 and Figure S33). Nitration of the phenyl group also occurs forming 2-(nitrophenyl)-*N*,*N*-di-*n*-octylacetamide (Figure 4, compound 16); this compound is only formed in the 3.0 HNO_3-

contacted environment (Figure S34). The compound is not observed until the dose reaches 300 kGy, increasing sharply at higher doses, behavior consistent with a secondary reaction.

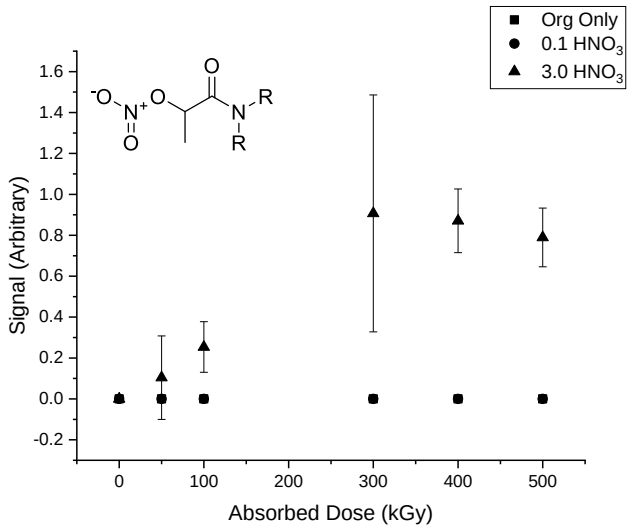

Figure 6: Normalized signal *vs.* absorbed dose for PhMeTODGA compound 14. This product could be formed from cleavage of the bond between the ether and the methyl-substituted methylene carbon in PhMeTODGA, followed by reaction with a nitrate radical. The corresponding compound for PhTODGA was not detected. The radical formed from the cleavage of this PhMeTODGA bond would initially be a secondary carbon-centered radical, as opposed to the primary carbon-centered radical that would be formed from cleavage of the analogous bond in PhTODGA.

In DHDPDGA, cleavage of the C_{CH2}—O_{ether} bond generates *N*-hexyl-*N*-phenyl glycolamide by H• capping of the initially formed O_{ether} radical (Figure S4, compound 6). The companion acetamide derivative is also observed in high abundance (Figure S4, compound 7). In the organic-only, and HNO_3-contacted organic environments, the abundances of both compounds increase by an order of magnitude over the first 50 kGy of gamma dose, and then display slower but steady increases at higher doses (Figure S58, Figure S59). In addition, capping of the methylene radical with a H_3C• results in formation of *N*-hexyl-*N*-phenyl propanamide, which is observed in abundance in the organic-only, and in the 0.1 M HNO_3-contacted organic environments (Figure S4, compound 12) after 50 kGy (Figure S61). Furthermore, double H_3C• addition also occurs, furnishing *N*-hexyl-2-methyl-*N*-phenyl

propanamide (Figure S4, compound 16) albeit at low abundance; the majority of the compound is formed over the first 50 kGy of gamma dose in the organic-only, and acid-contacted organic environments (Figure S61). The propanamide derivative also undergoes serial C_{phenyl}-H• cleavage with O_2NO• capping, to generate *N*-hexyl-*N*-(nitratophenyl) propanamide (Figure S62, compound 12 + NO_3). We note that an isomer, *N*-hexyl-2-methoxy-*N*-(nitrophenyl) acetamide, is also a possibility. This compound is observed in the third phase and is slowly formed with increasing dose in the organic acid-contacted environments (Figure S62).

The O_{ether} radical initially formed from DHDPDGA evidently undergoes oxidation, which combined with H_3C• capping furnishes *N*-hexyl-*N*-phenyl pyruvamide (Figure S4, compound 14). This compound is observed with modest abundance in the organic-only, third phase, and organic phase of the HNO_3-contacted experiments, before exposure to any radiation (Figure S63) and indicates that the compound is formed in a purely chemical fashion. The radiolysis profiles are either flat or show modest declines with increasing dose. It is hypothesized that DHDPDGA compound 14 would be formed from DHDPDGA compound 6, which is present in unirradiated DHDPDGA (Figure S58), likely as an impurity from synthesis.

Serial $C_{methylene}$—O_{ether} / C_{phenyl}—H• cleavages also occur in DHDPDGA, with nitrato radical capping on the phenyl moiety, to generate *N*-hexyl-*N*-(nitratophenyl) glycolamide (Figure S5, compound 6 + NO_3). This compound is most prevalent in the organic phase of the 0.1 M HNO_3-contacted experiment in the 100 – 300 kGy dose range; however, it is also observed in the third phase and in the organic-3.0 M HNO_3-contacted experiment (Figure S64). The formation of the compound mainly occurs during the first 100 kGy of gamma dose.

The primary DHDPDGA radiolysis product *N*-hexyl-*N*-phenyl glycolamide (DHDPDGA compound 6) also undergoes C_{phenyl}—H cleavage followed by O_2N• capping, to form *N*-

hexyl-*N*-(nitrophenyl) propanamide (Figure S65). This compound cannot be distinguished from *N*-hexyl-2-nitrato-*N*-phenylacetamide, or *N*-hexyl-*N*-(nitratophenyl)acetamide, based on elemental composition/exact mass measurement. The nitratoacetamide could be reasonably formed by C_{CH2}—O_{ether} cleavage with O_2NO• capping of the O_{ether} radical, and the nitratophenyl acetamide by C_{phenyl}—H• cleavage / O_2NO• capping. This compound is initially more abundant in the third phase before irradiation, indicating that it is at least partially formed by a non-radiolytic mechanism. However, its abundance increases dramatically over the first 50 kGy of gamma dose in the organic acid-contacted, and organic-only environments (Figure S65).

An analogous reaction involving nitro capping also occurs, forming *N*-hexyl-*N*-(nitrophenyl) acetamide (Figure S5, compound 7 + NO_2). Its formation is most favored in the organic phase of the 3 M HNO_3-contacted experiments, and it is also prevalent in the third phase. With increasing dose, its abundance quickly increases, followed by a slower increase over the entire dose range, suggesting formation by multiple radiolysis processes (Figure S66). Capping with ON• generates a related derivative, *N*-hexyl-*N*-(nitrosophenyl)acetamide (Figure S5, compound 7 + NO). The nitrosophenyl derivative is most abundant in the organic-only and organic acid-contacted experiments, with abundance increasing quickly at first, then continuing to increase with increasing gamma dose (Figure S67).

Additional Degradation Pathways

DHDPDGA undergoes radiolytic cleavage of H•, most likely from one of the hexyl chains, to form a radical that is an intermediate in reductive elimination of H_2 that generates *N*-hexyl-*N*-phenyl-*N'*-hexenyl-*N'*-phenyl diglycolamide (Figure S4, compound 13). The abundance of this compound increases by an order of magnitude within the first 50 kGy of gamma dose in the organic-only and organic phase of the 0.1 M HNO_3-contacted experiment (Figure S36). Cleavage of H• from the phenyl substituents is also occurring; the resulting phenyl-based

radical is capped with nitrogen oxide radicals, generating nitrophenyl (Figure S5, compound DHDPDGA + NO_2 and Figure S37) and nitratophenyl (Figure S5, compound DHDPDGA + NO_3 and Figure S38) derivatives of intact DHDPDGA. These radiolysis products are observed in the organic-only, organic HNO_3-contacted, and third phase environments, with abundances in general steadily increasing with increasing gamma dose.

Conclusions

The suite of detected degradation products reported here is significantly larger than in prior work, and while that is partially due to the asymmetry of these molecules, it is also due to the presence of several radiolytic mechanisms that have not previously been reported for diglycolamides. The degradation reactions can be categorized according to the four primary diglycolamide bonds that are broken: C_{alkyl}—N_{amide}, N_{amide}—$C_{C=O}$, $C_{C=O}$—C_{CH2}, and C_{CH2}—O_{ether}. Radicals formed by cleavage of these bonds are capped principally by H•, but also by HO•, H_3C•, O_2NO•, O_2N•, and ON•, to generate a wide range of products. Exact mechanisms are not known; however, the radiolysis profiles of the degradation products enable hypothesis of which are formed by primary degradation reactions, and which are from secondary reactions.

While some of these mechanisms appear to be directed by the presence of the phenyl group (primarily rapid oxidation of OH• radical addition adjacent to the phenyl group), most of the mechanisms should also be present for TODGA and other diglycolamides (CH_3• and nitrogen dioxide radical addition in particular). Thus, it is likely that the analogous degradation products of TODGA that would result from addition of CH_3• or nitrogen oxide radicals exist but have not been reported due to low abundance and/or the presence of other organic interferant molecules, either from the *n*-dodecane or from the sample analysis diluents or chromatographic mobile phase solvents. A complete understanding of the

radiation chemistry of fuel cycle ligands is necessary for construction of process models that will enable optimum process performance. Thus, the identification of these previously unreported radiolytic degradation mechanisms of diglycolamides suggests the radiation chemistry of previously studied diglycolamides that are currently candidates for advanced fuel reprocessing applications, specifically TODGA and its branched side -chain analog, *N*,*N*,*N'*,*N'*-tetra(2-ethylhexyl) diglycolamide, should be reexamined.

Given the plethora of degradation products identified for these diglycolamides, it is very likely that at least some of them would exert some effect on an actual separation process. While most of the degradation products identified here have not been directly studied, prior studies of the influence of similar degradation products can provide some clues about their possible behavior. The results of Galán et al.[27] suggest that degradation products of the phenyl-substituted DGAs studied here that are the result of loss of a single side chain (PhMeTODGA compounds 23a,b and 24a,b, PhTODGA compounds 19 and 20, and DHDPDGA compounds 1 and 2) would be expected to have distribution ratios greater than one for the trivalent actinides and lanthanides, and thus enhance extraction. Carboxylic acid-containing degradation products (PhMeTODGA compounds 9a,b and 11a,b, PhTODGA compounds 8 and 10, and DHDPDGA compound 9) would be expected to have distribution ratios less than one, and would inhibit extraction.

PhTODGA compound 7 is 2-hydroxy-N,N-dioctylacetamide, which has been shown to have distribution ratios greater than one for trivalent actinides and lanthanides.[27,28] It was suggested that the hydroxyl group contributes to extraction. Based on this, PhMeTODGA compounds 3 and 17, PhTODGA compounds 3 and 14, and DHDPDGA compound 4 would be expected to have distribution ratios greater than one. However, caution must be exercised; PhMeTODGA compound 7 is 2-hydroxy-N,N-dioctylpropanamide, which was shown by Hubscher-Bruder et al. to have distribution ratios less than one for the trivalent actinides and

lanthanides.[28] This compound only differs from 2-hydroxy-N,N-dioctylacetamide by a single methyl (CH_3) group, which shows how small structural changes can have a large effect on extraction behavior. PhMeTODGA compound 8 and PhTODGA compound 9 are both N,N-dioctylformamide; Hubscher-Bruder et al. saw little influence on extraction from this compound.[28] PhMeTODGA compound 10 and PhTODGA compound 11 are both N,N-dioctylacetamide; Hubscher-Bruder et al. measured distribution ratios greater than one for zirconium and palladium, which would decrease the selectivity of a process for extracting the trivalent actinides and lanthanides.[28] As with the hydroxylated compounds, small structural changes can have large effects on extraction behavior.

It is difficult to speculate the influence of other degradation products that have not been previously studied, since degradation product extraction behavior can change significantly with only small changes in structure. Given the large number of identified degradation products, it would be challenging to measure the influence of all the products that have not been previously studied. Since the DGAs studied here have lower distribution ratios for trivalent actinides and lanthanides, less radiation resistance, and produce more degradation products than TODGA, it is unlikely that they will find use in an actual separation process.

Acknowledgements

The gamma-ray irradiation and UHPLC-ESI-MS experiments performed at Idaho National Laboratory were supported by the US Department of Energy (US-DOE), Assistant Secretary for Nuclear Energy, under the Fuel Cycle R&D Program, Idaho Operations Office Contract DE-AC07-05ID14517. Additional financial support for this research was provided by the

European Commission: projects SACSESS and GENIORS, Grant No. 323282 and 755171, respectively.

Disclosure Statement

The authors report there are no competing interests to declare.

References

[1] IEA. *Net Zero by 2050 - A Roadmap for the Global Energy Sector*; IEA: Paris, France, 2021.
[2] Todd, T. A. Separations Research for Advanced Nuclear Fuel Cycles. In *Nuclear Energy and the Environment*; ACS Symposium Series; American Chemical Society, 2010; Vol. 1046, pp 13–18, DOI: 10.1021/bk-2010-1046.ch002.
[3] *Management of Spent Nuclear Fuel and Its Waste*; The European Academies' Science Advisory Counsil (ESAC): Brussels, Belgium, 2014; pp 1–40.
[4] Wigeland, R. A.; Bauer, T. H.; Fanning, T. H.; Morris, E. E. Separations and Transmutation Criteria to Improve Utilization of a Geologic Repository. *Nuclear Technology* **2006**, *154* (1), 95–106, DOI: 10.13182/NT06-3.
[5] Poinssot, Ch.; Bourg, S.; Ouvrier, N.; Combernoux, N.; Rostaing, C.; Vargas-Gonzalez, M.; Bruno, J. Assessment of the Environmental Footprint of Nuclear Energy Systems. Comparison between Closed and Open Fuel Cycles. *Energy* **2014**, *69*, 199–211, DOI: 10.1016/j.energy.2014.02.069.
[6] Serp, J.; Poinssot, C.; Bourg, S. Assessment of the Anticipated Environmental Footprint of Future Nuclear Energy Systems. Evidence of the Beneficial Effect of Extensive Recycling. *Energies* **2017**, *10* (9), DOI: 10.3390/en10091445.
[7] NEA. *Potential Benefits and Impacts of Advanced Nuclear Fuel Cycles with Actinide Partitioning and Transmutation*; OECD Publishing: Paris, France, 2011.
[8] Magill, J.; Berthou, V.; Haas, D.; Galy, J.; Schenkel, R.; Wiese, H.-W.; Heusener, G.; Tommasi, J.; Youinou, G. Impact Limits of Partitioning and Transmutation Scenarios on the Radiotoxicity of Actinides in Radioactive Waste. *Nuclear Energy* **2003**, *42* (5), 263–277.
[9] Geist, A.; Adnet, J.-M.; Bourg, S.; Ekberg, C.; Galán, H.; Guilbaud, P.; Miguirditchian, M.; Modolo, G.; Rhodes, C.; Taylor, R. An Overview of Solvent Extraction Processes Developed in Europe for Advanced Nuclear Fuel Recycling, Part 1 — Heterogeneous Recycling. *Separation Science and Technology* **2021**, *56* (11), 1866–1881, DOI: 10.1080/01496395.2020.1795680.
[10] Lyseid Authen, T.; Adnet, J.-M.; Bourg, S.; Carrott, M.; Ekberg, C.; Galán, H.; Geist, A.; Guilbaud, P.; Miguirditchian, M.; Modolo, G.; et al. An Overview of Solvent Extraction Processes Developed in Europe for Advanced Nuclear Fuel Recycling, Part 2 — Homogeneous Recycling. *Separation Science and Technology* **2022**, *57* (11), 1724–1744, DOI: 10.1080/01496395.2021.2001531.
[11] Mincher, B. J.; Modolo, G.; Mezyk, S. P. Review Article: The Effects of Radiation Chemistry on Solvent Extraction: 1. Conditions in Acidic Solution and a Review of TBP

Radiolysis. *Solvent Extr. Ion Exch.* **2009**, *27* (1), 1–25, DOI: 10.1080/07366290802544767.
[12] Mincher, B. J.; Modolo, G.; Mezyk, S. P. Review Article: The Effects of Radiation Chemistry on Solvent Extraction: 2. A Review of Fission-Product Extraction. *Solvent Extr. Ion Exch.* **2009**, *27* (3), 331–353, DOI: 10.1080/07366290902821263.
[13] Mincher, B. J.; Modolo, G.; Mezyk, S. P. Review Article: The Effects of Radiation Chemistry on Solvent Extraction 3: A Review of Actinide and Lanthanide Extraction. *Solvent Extr. Ion Exch.* **2009**, *27* (5–6), 579–606, DOI: 10.1080/07366290903114098.
[14] Mincher, B. J. Chapter 8 - Radiation Chemistry in the Reprocessing and Recycling of Spent Nuclear Fuels. In *Reprocessing and Recycling of Spent Nuclear Fuel*; Taylor, R., Ed.; Woodhead Publishing: Oxford, 2015; pp 191–211.
[15] Ansari, S. A.; Pathak, P.; Mohapatra, P. K.; Manchanda, V. K. Aqueous Partitioning of Minor Actinides by Different Processes. *Separation & Purification Reviews* **2011**, *40* (1), 43–76, DOI: 10.1080/15422119.2010.545466.
[16] Ansari, S. A.; Pathak, P.; Mohapatra, P. K.; Manchanda, V. K. Chemistry of Diglycolamides: Promising Extractants for Actinide Partitioning. *Chem. Rev.* **2012**, *112* (3), 1751–1772, DOI: 10.1021/cr200002f.
[17] Sugo, Y.; Sasaki, Y.; Tachimori, S. Studies on Hydrolysis and Radiolysis of N,N,N′,N′-Tetraoctyl-3-Oxapentane-1,5-Diamide. *Radiochim. Acta* **2002**, *90* (3), DOI: 10.1524/ract.2002.90.3_2002.161.
[18] Zarzana, C. A.; Groenewold, G. S.; Mincher, B. J.; Mezyk, S. P.; Wilden, A.; Schmidt, H.; Modolo, G.; Wishart, J. F.; Cook, A. R. A Comparison of the γ-Radiolysis of TODGA and T(EH)DGA Using UHPLC-ESI-MS Analysis. *Solvent Extr. Ion Exch.* **2015**, *33* (5), 431–447, DOI: 10.1080/07366299.2015.1012885.
[19] Kimberlin, A.; Guillaumont, D.; Arpigny, S.; Camès, B.; Guilbaud, P.; Saint-Louis, G.; Galán, H.; Berthon, L. An Experimental and Computational Look at the Radiolytic Degradation of TODGA and the Effect on Metal Complexation. *New J. Chem.* **2021**, *45* (28), 12479–12493, DOI: 10.1039/D1NJ01143J.
[20] Kimberlin, A.; Saint-Louis, G.; Guillaumont, D.; Camès, B.; Guilbaud, P.; Berthon, L. Effect of Metal Complexation on Diglycolamide Radiolysis: A Comparison between Ex Situ Gamma and in Situ Alpha Irradiation. *Phys. Chem. Chem. Phys.* **2022**, *24* (16), 9213–9228, DOI: 10.1039/D1CP05731F.
[21] Sharma J. N.; Ruhela R.; Singh K. K.; Kumar Manoj; Janardhanan C.; Achutan P. V.; Manohar S.; Wattal P. K.; Suri A. K. Studies on Hydrolysis and Radiolysis of Tetra(2-Ethylhexyl)Diglycolamide (TEHDGA)/Isodecyl Alcohol/n-Dodecane Solvent System. *Radiochim. Acta* **2010**, *98* (8), 485, DOI: 10.1524/ract.2010.1749.
[22] Galán, H.; Zarzana, C. A.; Wilden, A.; Nunez, A.; Schmidt, H.; Egberink, R. J. M.; Leoncini, A.; Cobos, J.; Verboom, W.; Modolo, G.; et al. Gamma-Radiolytic Stability of New Methylated TODGA Derivatives for Minor Actinide Recycling. *Dalton Trans.* **2015**, *44* (41), 18049–18056, DOI: 10.1039/C5DT02484F.
[23] Roscioli-Johnson, K. M.; Zarzana, C. A.; Groenewold, G. S.; Mincher, B. J.; Wilden, A.; Schmidt, H.; Modolo, G.; Santiago-Schübel, B. A Study of the γ-Radiolysis of N,N-Didodecyl-N′,N′-Dioctyldiglycolamide Using UHPLC-ESI-MS Analysis. *Solvent Extr. Ion Exch.* **2016**, *34* (5), 439–453, DOI: 10.1080/07366299.2016.1212540.
[24] Verlinden, B.; Van Hecke, K.; Wilden, A.; Hupert, M.; Santiago-Schübel, B.; Egberink, R. J. M.; Verboom, W.; Kowalski, P. M.; Modolo, G.; Verwerft, M.; et al. Gamma Radiolytic Stability of the Novel Modified Diglycolamide 2,2′-Oxybis(N,N-Didecylpropanamide) (MTDDGA) for Grouped Actinide Extraction. *RSC Adv.* **2022**, *12* (20), 12416–12426, DOI: 10.1039/D1RA08761D.

[25] Koubský, T.; Fojtíková, J.; Kalvoda, L. Radical Degradation Stability of Ether Linkage in N,N,N′,N′-Tetraoctyldiglycolamide and Related Organic Extractants: A Density Functional Study. *Progress in Nuclear Energy* **2017**, *94*, 208–215, DOI: 10.1016/j.pnucene.2016.07.010.
[26] Koubský, T.; Luštinec, J. Application of Quantum Mechanical Simulations for Studying the Radiolytic Stability of Prospective Extractants in the Nuclear Fuel Cycle. *Journal of Radioanalytical and Nuclear Chemistry* **2018**, *318* (3), 2407–2413, DOI: 10.1007/s10967-018-6225-2.
[27] Galán, H.; Núñez, A.; Espartero, A. G.; Sedano, R.; Durana, A.; Mendoza, J. de. Radiolytic Stability of TODGA: Characterization of Degraded Samples under Different Experimental Conditions. *Procedia Chem.* **2012**, *7*, 195–201, DOI: 10.1016/j.proche.2012.10.033.
[28] Hubscher-Bruder, V.; Mogilireddy, V.; Michel, S.; Leoncini, A.; Huskens, J.; Verboom, W.; Galán, H.; Núñez, A.; Cobos, J.; Modolo, G.; et al. Behaviour of the Extractant Me-TODGA upon Gamma Irradiation: Quantification of Degradation Compounds and Individual Influences on Complexation and Extraction. *New J. Chem.* **2017**, *41* (22), 13700–13711, DOI: 10.1039/C7NJ02136D.
[29] Zarzana, C. A.; McAlpine, J.; White, A.; Rae, C.; Wilden, A.; Hupert, M.; Stärk, A.; Iqbal, M.; Verboom, W.; Mincher, B. J.; et al. Gamma Radiolysis of Phenyl-Substituted TODGAs: Part I. *PLACEHOLDER*.
[30] Sánchez-García, Iván; Galán, Hitos; Perlado, Jose Manuel; Cobos, Joaquín. Stability Studies of GANEX System under Different Irradiation Conditions. *EPJ Nuclear Sci. Technol.* **2019**, *5*, 19, DOI: 10.1051/epjn/2019049.
[31] Wilden, A.; Mincher, B. J.; Mezyk, S. P.; Twight, L.; Roscioli-Johnson, K. M.; Zarzana, C. A.; Case, M. E.; Hupert, M.; Stärk, A.; Modolo, G. Radiolytic and Hydrolytic Degradation of the Hydrophilic Diglycolamides. *Solvent Extr. Ion Exch.* **2018**, *36* (4), 1–13, DOI: 10.1080/07366299.2018.1495384.
[32] Iqbal, M.; Huskens, J.; Verboom, W.; Sypula, M.; Modolo, G. Synthesis and Am/Eu Extraction of Novel TODGA Derivatives. *Supramol. Chem.* **2010**, *22* (11–12), 827–837, DOI: 10.1080/10610278.2010.506553.
[33] Leoncini, A.; Huskens, J.; Verboom, W. Preparation of Diglycolamides via Schotten–Baumann Approach and Direct Amidation of Esters. *Synlett* **2016**, *27* (17), 2463–2466, DOI: 10.1055/s-0035-1561495.
[34] Fricke, H.; Hart, E. J. The Oxidation of Fe++ to Fe+++ by the Irradiation with X-Rays of Solutions of Ferrous Sulfate in Sulfuric Acid. *J. Chem. Phys.* **1935**, *3* (1), 60–61, DOI: 10.1063/1.1749558.
[35] Sehested, K. The Fricke Dosimeter. In *Manual on Radiation Dosimetry*; Holm, N. W., Berry, R. J., Eds.; Marcel Dekker, Inc: New York, 1970; pp 313–317.